Atmospheric
Measurement
Techniques

A new method for atmospheric detection of the CH$_3$O$_2$ radical

Lavinia Onel[1], **Alexander Brennan**[1], **Paul W. Seakins**[1,2], **Lisa Whalley**[1,2], **and Dwayne E. Heard**[1,2]

[1]School of Chemistry, University of Leeds, Leeds, LS2 9JT, UK
[2]National Centre for Atmospheric Science, University of Leeds, LS2 9JT, UK

Correspondence to: Lavinia Onel (chmlo@leeds.ac.uk) and Dwayne Heard (d.e.heard@leeds.ac.uk)

Abstract. A new method for measurement of the methyl peroxy (CH$_3$O$_2$) radical has been developed using the conversion of CH$_3$O$_2$ into CH$_3$O by excess NO with subsequent detection of CH$_3$O by fluorescence assay by gas expansion (FAGE) with laser excitation at ca. 298 nm. The method can also directly detect CH$_3$O, when no nitric oxide is added. Laboratory calibrations were performed to characterise the FAGE instrument sensitivity using the conventional radical source employed in OH calibration with conversion of a known concentration of OH into CH$_3$O$_2$ via reaction with CH$_4$ in the presence of O$_2$. Detection limits of 3.8×10^8 and 3.0×10^8 molecule cm^{-3} were determined for CH$_3$O$_2$ and CH$_3$O respectively for a signal-to-noise ratio of 2 and 5 min averaging time. Averaging over 1 h reduces the detection limit for CH$_3$O$_2$ to 1.1×10^8 molecule cm^{-3}, which is comparable to atmospheric concentrations. The kinetics of the second-order decay of CH$_3$O$_2$ via its self-reaction were observed in HIRAC (Highly Instrumented Reactor for Atmospheric Chemistry) at 295 K and 1 bar and used as an alternative method of calibration to obtain a calibration constant with overlapping error limits at the 1σ level with the result of the conventional method of calibration. The overall uncertainties of the two methods of calibrations are similar – 15 % for the kinetic method and 17 % for the conventional method – and are discussed in detail. The capability to quantitatively measure CH$_3$O in chamber experiments is demonstrated via observation in HIRAC of CH$_3$O formed as a product of the CH$_3$O$_2$ self-reaction.
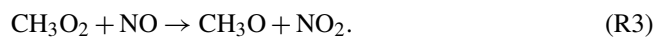
1 Introduction

Methyl peroxy (CH$_3$O$_2$) radicals are critical intermediates in the atmospheric oxidation (Orlando and Tyndall, 2012) and combustion of hydrocarbons (Zador et al., 2011). In the remote atmosphere, CH$_3$O$_2$ is mainly formed by the reaction of methane with the OH radical via abstraction of an H atom (Reaction R1), followed by the reaction of the produced CH$_3$ radical with O$_2$ (Reaction R2).

$$\text{OH} + \text{CH}_4 \rightarrow \text{CH}_3 + \text{H}_2\text{O} \tag{R1}$$

$$\text{CH}_3 + \text{O}_2 + \text{M} \rightarrow \text{CH}_3\text{O}_2 + \text{M} \tag{R2}$$

Methyl peroxy radicals can also be formed from more complex species, e.g. the reaction of acetyl peroxy radicals with HO$_2$ in low-NO$_x$ environments or the reaction of acetyl peroxy radicals with NO in anthropogenically influenced environments. CH$_3$O$_2$ is predicted to be the most abundant peroxy radical in the atmosphere, yet there are no specific measurements of its concentration. Daytime concentrations estimated using a box model utilising the MCM (Master Chemical Mechanism) version 3.3.1 (Saunders et al., 2003; Jenkin et al., 2015) are $\sim 6 \times 10^8$ molecule cm^{-3} in the tropical Atlantic Ocean in summer (Whalley et al., 2010), $\sim 2 \times 10^8$ molecule cm^{-3} in a tropical rainforest (Whalley et al., 2011) and lower in polluted environments, for example $\sim 5 \times 10^7$ molecule cm^{-3} in London in summertime (Whalley et al., 2017).

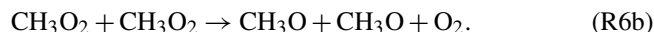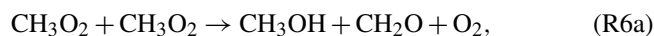The reaction of CH$_3$O$_2$ with NO (Reaction R3) usually dominates the chemistry of CH$_3$O$_2$, particularly in environments influenced by anthropogenic NO$_x$ emissions, resulting in NO$_2$ production and hence ozone production:

$$CH_3O_2 + NO \rightarrow CH_3O + NO_2. \quad \text{(R3)}$$

The subsequent reaction of CH_3O with O_2 (Reaction R4) produces HO_2, which in turn oxidises another NO to NO_2 (Reaction R5) with further production of O_3 and propagation of the HO_x radical chain:

$$CH_3O + O_2 \rightarrow CH_2O + HO_2, \quad \text{(R4)}$$
$$HO_2 + NO \rightarrow OH + NO_2. \quad \text{(R5)}$$
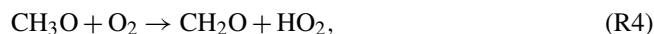
However, under low NO_x levels (e.g. remote forested environments and the marine boundary layer), the self-reaction of CH_3O_2 (Reaction R6) and the reactions of CH_3O_2 with HO_2 and other organic peroxy (RO_2) species are important radical removal/termination reactions. The CH_3O_2 self-reaction occurs through two channels, Reactions (R6a) and (R6b) (Tyndall et al., 1998):

$$CH_3O_2 + CH_3O_2 \rightarrow CH_3OH + CH_2O + O_2, \quad \text{(R6a)}$$
$$CH_3O_2 + CH_3O_2 \rightarrow CH_3O + CH_3O + O_2. \quad \text{(R6b)}$$

Despite the importance of Reaction (R6), there are uncertainties of about a factor of 2 in the value of its rate coefficient at room temperature, k_6, which has a range of $(2.7–5.2) \times 10^{-13}$ cm^3 molecule^{-1} s^{-1} (Atkinson et al., 2006); the preferred IUPAC value is $k_6 = 3.5 \times 10^{-13}$ cm^3 molecule^{-1} s^{-1}. The previous kinetic studies used time-resolved UV-absorption spectroscopy to detect CH_3O_2 radical, typically at 250 nm, (Sander and Watson, 1980, 1981; McAdam et al., 1987; Kurylo and Wallington, 1987; Jenkin et al., 1988; Simon et al., 1990; Lightfoot et al., 1990). UV-absorption spectroscopy is a relatively insensitive technique and hence the detection limits of CH_3O_2 were quite high, for example approximately 4×10^{12} molecule cm^{-3} (Sander and Watson, 1980, 1981). In addition, due to the broad, featureless spectra of RO_2 species, which often overlap, UV absorption is a relatively unselective technique for the study of the kinetics of individual RO_2. Therefore, there is a clear need for the determination of k_6 using a more selective method, which will be addressed in subsequent studies.

At present, CH_3O_2 is not specifically measured in the atmosphere by any direct or indirect method. Time-resolved continuous-wave cavity ring-down spectroscopy (CRDS), using the ν_{12} transition of the $A \leftarrow X$ band at ~ 1.3 µm, has been used to detect CH_3O_2 directly in a photoreactor (Farago et al., 2013; Bossolasco et al., 2014). However, the detection limit is not sufficiently sensitive to enable tropospheric detection. Typically, the sum of HO_2 and all organic RO_2 has been measured in the atmosphere, making no distinction between HO_2 and different RO_2 species, although more recently the sum of RO_2 has been quantified separately from HO_2. One of the methods uses chemical ionisation mass spectrometry to determine the sum $[HO_2] + \sum_i[RO_{2,i}]$ or separately $[HO_2]$,

depending on the control of the flows of the NO and SO_2 reagents (Hanke et al., 2002; Edwards et al., 2003). The sum $[HO_2] + \sum_i[RO_{2,i}]$ has also been determined for many years by the peroxy radical chemical amplifier (PERCA) method, which uses NO and CO to generate NO_2 amplified by a chain reaction, and subsequently measured by a variety of methods, for example luminol fluorescence, laser-induced fluorescence (LIF) or cavity absorption methods (Cantrell and Stedman, 1982; Cantrell et al., 1984; Miyazaki et al., 2010; Hernandez et al., 2001; Green et al., 2006; Chen et al., 2016). A modification of PERCA, using a denuder to remove HO_2 has been used to estimate the sum of RO_2 (Miyazaki et al., 2010). RO_xLIF is a more recent method, which uses OH LIF detection at low pressure, known as FAGE (fluorescence assay by gas expansion) (Fuchs et al., 2008; Whalley et al., 2013). The RO_xLIF method measures either $[HO_x] = [OH] + [HO_2]$, by converting HO_x into HO_2 through addition of CO, or $[RO_x] = [HO_x] + \sum_i([RO_{2,i}] + [RO_i])$, by titrating RO_x to HO_2 by added NO and CO. After the conversion into HO_2, HO_2 is converted into OH in the FAGE chamber and detected by LIF. The sum $\sum_i[RO_{2,i}]$ and the concentration of the initial HO_2 can be determined from the separate measurements of HO_x, RO_x and OH. The limit of detection (LOD) of the RO_xLIF method is ~ 0.1 pptv (2.5×10^6 molecule cm^{-3}) (Fuchs et al., 2008; Whalley et al., 2013). Recently, the interference from certain types of RO_2 radicals in the FAGE detection of HO_2 was deliberately exploited to enable a partial RO_2 speciation (Whalley et al., 2013). The method was used in the Clean Air for London campaign (ClearfLo) to distinguish between the sum of alkene, aromatic, and long-chain alkane-derived RO_2 radicals and the sum of short-chain alkane-derived RO_2 radicals (Whalley et al., 2013).

As methoxy (CH_3O) radicals can be generated by techniques such as pulsed laser photolysis and microwave discharge and detected with high sensitivity by LIF (Shannon et al., 2013; Chai et al., 2014; Albaladejo et al., 2002; Biggs et al., 1993, 1997), the method has been used in kinetic studies of a range of CH_3O reactions. These studies used the electronic excitation of the methoxy radical from the ground state to the first electronically excited state ($A^2A_1 \leftarrow X^2E$). The $A \leftarrow X$ excitation spectrum covers the range $\sim 275–317$ nm and leads to fluorescence from several vibronic bands in the near UV, which has been reported in a series of experimental and theoretical studies (Inoue et al., 1980; Kappert and Temps, 1989; Powers et al., 1997; Nagesh et al., 2014).

This paper reports the development of a new method for the selective and sensitive detection of CH_3O_2 radicals using FAGE by titrating CH_3O_2 to CH_3O by reaction with added NO (Reaction R3) and then detecting the resultant CH_3O by off-resonant LIF with laser excitation at ca. 298 nm. The method is similar to the standard method used for the detection of HO_2 radicals by FAGE through conversion of HO_2 to OH by reaction with added NO followed by OH on-

resonance LIF at about 308 nm (Heard and Pilling, 2003). As LIF is not an absolute detection method, FAGE instruments require calibration, with the 184.9 nm photolysis of water vapour in air using a mercury (Hg) Pen-Ray lamp being a common method employed for generating known concentrations of OH and HO$_2$ (Heard and Pilling, 2003):

$$H_2O \xrightarrow{184.9\,nm} OH + H, \tag{R7}$$

$$H + O_2 + M \rightarrow HO_2 + M, \tag{R8}$$

where $M = N_2$, O_2 and the photodissociation quantum yield of OH and H is unity. In this study the photolysis of water vapour is performed in the presence of excess methane to produce CH$_3$O$_2$:

$$CH_4 + OH \rightarrow CH_3 + H_2O, \tag{R1}$$

$$CH_3 + O_2 + M \rightarrow CH_3O_2 + M. \tag{R2}$$

An alternative CH$_3$O$_2$ calibration is also presented, consisting of the analysis of the kinetics of the CH$_3$O$_2$ decay by self-reaction monitored by FAGE and compared with the water photolysis method. The studies are performed within HIRAC (Highly Instrumented Reactor for Atmospheric Chemistry), which is a 2.25 m^3, custom-built, stainless steel chamber simulating the ambient conditions (Glowacki et al., 2007). HIRAC has been used in alternative calibrations of FAGE for OH and HO$_2$ using the temporal evolution of appropriate species, in validation and development of new atmospheric measurement techniques as well as in kinetic and mechanistic studies of atmospheric relevant reactions (Malkin et al., 2010; Winiberg et al., 2015, 2016).

Direct LIF detection of CH$_3$O radicals, which is also a key intermediate in the oxidation of methane and other volatile organic compounds (VOCs) in the troposphere and formed by reactions such as Reactions (R3) and (R6b), is also reported here. However, in the atmosphere, CH$_3$O is exclusively consumed by reaction with O$_2$ (Reaction R4) generating formaldehyde and recycling HO$_2$, resulting in a very short lifetime and consequently very low concentration ($\sim 10^2$–10^3 molecule cm^{-3}). For this reason no measurements in the atmosphere have previously been attempted. The photolysis of CH$_3$OH at 184.9 nm is used to estimate the FAGE sensitivity for CH$_3$O. The dominant photolysis channel of methanol between 165 and 200 nm generates CH$_3$O radicals (Wen et al., 1994; Kassab et al., 1983; Marston et al., 1993):

$$CH_3OH \xrightarrow{165-200\,nm} CH_3O + H. \tag{R9}$$
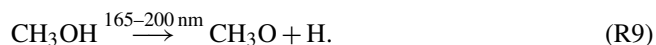
A photodissociation quantum yield of CH$_3$O of 0.86 ± 0.10 has been found at 193.3 nm (Satyapal et al., 1989) in qualitative agreement with analysis of the end-products of the methanol photodissociation at 184.9 nm (Porter and Noyes, 1959; Buenker et al., 1984). Here we report the first measurements of CH$_3$O concentrations in an atmospheric simulation

chamber. Methoxy radicals are generated by the CH$_3$O$_2$ self-reaction carried out within HIRAC at 295 K and 1000 mbar of N$_2$ containing O$_2$ in trace amounts to reduce the rate of removal of CH$_3$O by reaction with O$_2$. This work enhances the capability of HIRAC to measure short-lived radical species by the addition of both CH$_3$O$_2$ and CH$_3$O detection, and we discuss the potential of the method for detection of CH$_3$O$_2$ in the atmosphere itself.

2 Experimental

2.1 The FAGE instrument

Details on the HIRAC-based FAGE instrument for the detection of OH and HO$_2$ has been presented previously (Winiberg et al., 2015). Figure 1 shows a schematic cross section of the instrument inlet and the two fluorescence detection cells. The gas was sampled with a flow rate of 3.2 slm through a 1 mm diameter pinhole and passed down a 50 mm diameter flow tube of 280 mm length first into the OH detection axis and, after a further 300 mm, into the CH$_3$O$_2$ detection axis. The pressure in the detection cells was maintained at 2.65 ± 0.05 Torr by using a high-capacity rotary-backed Roots blower pumping system (Leybold, Trivac D40B and Ruvac WAU251). CH$_3$O$_2$ radicals were titrated to CH$_3$O by adding high purity NO (BOC, N2.5 nitric oxide) with a typical 2.5 sccm flow rate (further details in Sect. 2.2) ~ 25 mm before the second detection axis into the centre of the flow. The resultant CH$_3$O radicals were measured by LIF.

Probe laser light was generated by an Nd:YAG (JDSU Q201-HD) pumped dye laser (Sirah Credo-Dye-N) using a DCM dye (Sirah) in ethanol and operating at a 5 kHz pulse repetition frequency, with a pulse width at half maximum height of 25 ns, typical pulse energy of 120 µJ pulse^{-1} and a linewidth of 0.08 cm^{-1} at 595 nm. The frequency doubled light at either ~ 308 nm (OH detection) or ~ 298 nm (CH$_3$O detection) was focused into fibre optic cables to be delivered to the two detection cells. OH and CH$_3$O radicals were separately detected by LIF spectroscopy by exciting at 307.99 nm using the Q$_1$(2) rotational line of the $A^2\sum^+ (\nu' = 0) \leftarrow X^2\Pi_i (\nu'' = 0)$ OH transition in the first detection axis to monitor on-resonant fluorescence (308.8 ± 5.0 nm) and excitation at 297.79 nm in the $A^2A_1 (\nu'_3 = 3) \leftarrow X^2E (\nu''_3 = 0)$ CH$_3$O transition in the second detection axis to monitor red-shifted off-resonant LIF (320–430 nm). Here ν_3 refers to the C–O stretching vibrational mode of CH$_3$O which demonstrates a progression in the LIF spectrum (Inoue et al., 1980; Kappert and Temps, 1989; Powers et al., 1997; Nagesh et al., 2014). The fluorescence in the two cells was collected orthogonal to the gas flow by two microchannel plate photomultiplier tubes (MCP-PMT) (Photek PMT325/Q/BI/G) equipped with a 50 ns gate unit (Photek GM10-50) for gated photon counting, and the signal was amplified using a pre-amplifier (Photek PA200-10). Further details on the OH de-
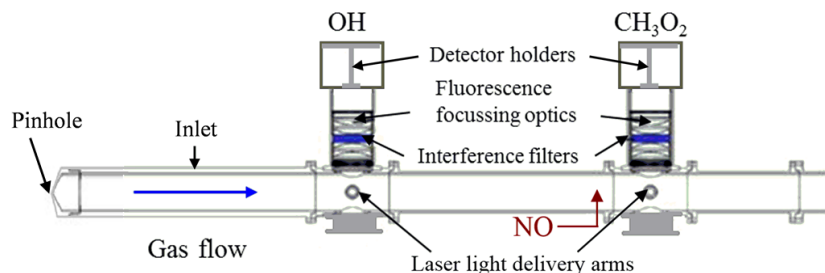
Figure 1. Vertical cross section of the FAGE fluorescence cells. The first (left) fluorescence cell was used to detect OH fluorescence through a 308.8 ± 5.0 nm bandpass filter (transmission $> 50\%$) and the second cell to detect CH$_3$O$_2$ after titration with added NO to form CH$_3$O using a bandpass filter between 320 and 430 nm with an average transmission $> 80\%$.

tection and calibration in HIRAC have been reported previously (Winiberg et al., 2015).

The laser and photon-counting timing for CH$_3$O detection was controlled by a delay pulse generator (9520 series, Quantum Composers). The relatively broad bandpass filter used for the collection of the CH$_3$O fluorescence (average transmission $> 80\%$ between 320 and 430 nm) allowed some red-shifted scattered light (presumably from the walls of the chamber) generated by the probe laser to be transmitted and hence detected by the MCP-PMT. In order to ameliorate this and reduce the background signal, the gate unit was opened 100 ns after the laser pulse to detect fluorescence integrated over a gate width of 2 µs. The optimum gate width of 2 µs (values in the range 1–3 µs were compared) is consistent with the CH$_3$O fluorescence lifetimes, calculated to be in the range of 0.9–1.5 µs, using the reported radiative lifetimes for CH$_3$O of 1.5 µs (Inoue et al., 1979), 2.2 µs (Ebata et al., 1982), and 4 ± 2 µs (Wendt and Hunziker, 1979) and using the fluorescence quenching rate coefficients of N$_2$ and O$_2$ (Wantuck et al., 1987) to calculate the rate of quenching at the pressure in the FAGE detection cell (2.65 ± 0.05 Torr). As the fluorescence lifetime of CH$_3$O(A) in the detection cell was 0.9–1.5 µs, delaying the counting of the fluorescence by 100 ns makes very little difference ($\sim 10\%$) in the fraction of fluorescence collected.

All LIF signals reported here were normalized to the probe laser power as measured with a laser power meter (Maestro, Gentec-EO) before the start of each LIF measurement. Fluctuations in the relative laser power were monitored via a photodiode (UDT-555UV, Laser Components) during the measurements and were accounted for in the signal normalisation. The LIF spectrum was corrected for the laser-scattered background by subtracting the normalized offline signal recorded over 60 s at the end of each LIF measurement using an offline wavelength $\lambda(\text{offline} = 300.29\,\text{nm}) = \lambda(\text{online} = 297.79\,\text{nm}) + 2.5$ nm, well away from any CH$_3$O absorption. The signals were large enough that during conditions where CH$_3$O$_2$ concentrations were constant (e.g. in calibrations or during HIRAC experiments where steady-state concentrations were generated) it was established that the

laser wavelength was stable over a long period once the laser wavelength had been tuned to the CH$_3$O transition. Hence, the online wavelength position for CH$_3$O fluorescence detection was found without using a reference cell. We are in the process of developing a reference cell for field measurements in the future, when the atmospheric concentrations of CH$_3$O$_2$ (and hence CH$_3$O after conversion) will be both lower and more variable over short timescales. Figure 2 shows the laser excitation spectrum centred at ~ 298 nm in the ν_3 vibronic band recorded using an increment of $\Delta\lambda = 10^{-3}$ nm. The spectrum agrees well with previous work (Inoue et al., 1980; Kappert and Temps, 1989; Shannon et al., 2013). Figure 3 shows typical laser excitation scans performed over a narrower range of wavelengths in order to locate $\lambda(\text{online})$. The LIF spectra were obtained by using the CH$_3$O or CH$_3$O$_2$ radicals generated in a flow tube described in Sect. 2.3.1, with the flow-tube output impinged close to the FAGE sampling inlet. The radicals were generated using the 184.9 nm light output of a Hg Pen-Ray lamp by either the photolysis of methanol in nitrogen to generate CH$_3$O or the photolysis of water vapour in synthetic air (to generate OH) in the presence of methane to form CH$_3$O$_2$. The CH$_3$O radicals were directly detected, while the CH$_3$O$_2$ radicals were first converted to CH$_3$O species by added NO prior to the fluorescence detection cell (Fig. 1). Similar laser scans to the scans shown in Fig. 3 were recorded by using the CH$_3$O$_2$ radicals produced in a steady-state concentration in HIRAC using photolytic mixtures of Cl$_2$–CH$_4$–air as described in Sect. 2.3.2. There were no unexpected features in the laser scans recorded when FAGE sampled CH$_3$O$_2$ radicals from HIRAC, consistent with no interference being anticipated in the FAGE measurements of CH$_3$O as there were no other species in HIRAC absorbing at 298 nm and fluorescing at the wavelengths transmitted by the bandpass filter (average transmission $> 80\%$ over 320–430 nm).

2.2 Optimisation of the NO concentration for methyl peroxy radical detection

As NO was added ~ 25 mm prior the methoxy detection axis (Fig. 1), some of the methoxy radicals formed by Re-
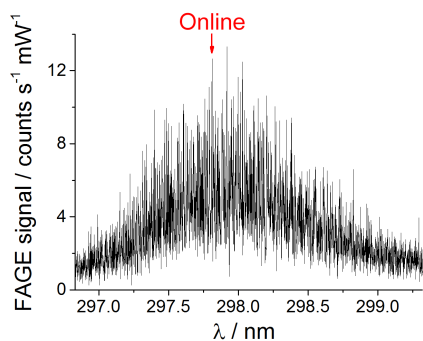
Figure 2. Laser excitation spectrum of the A^2A_1 ($v'_3 = 3$) ← X^2E ($v''_3 = 0$) transition of the methoxy radical. CH$_3$O radicals were obtained by photolysis of methanol in N$_2$ at 184.9 nm. Fluorescence cell pressure = 2.65 ± 0.05 Torr; wavelength increment $\Delta\lambda = 10^{-3}$ nm, with each point corresponding to 5000 laser shots. The red arrow indicates the wavelength λ(online) ~ 297.79 nm used for the time-resolved kinetic studies of CH$_3$O$_2$.
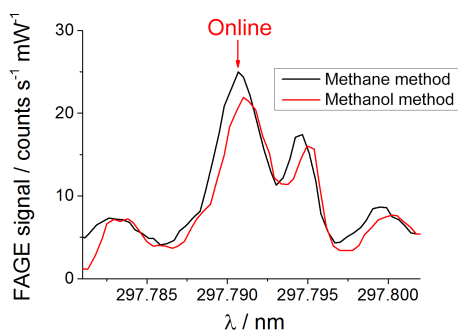

Figure 3. Typical laser excitation scans of CH$_3$O performed over a much smaller range of wavelengths. Methoxy radicals were generated using OH and CH$_4$ (black line) to produce 5.5×10^{10} molecule cm^{-3} CH$_3$O$_2$, subsequently titrated to CH$_3$O by adding NO, and the photolysis of methanol (red line) to generate 4.9×10^{10} molecule cm^{-3} CH$_3$O directly. See main text for the description of the methods and calibration. The signal was normalised for the laser power (10.3 ± 0.3 mW in the methane method and 8.7 ± 0.2 mW in the methanol method). Fluorescence cell pressure = 2.65 ± 0.05 Torr; wavelength increment $\Delta\lambda = 10^{-3}$ nm, with each point corresponding to 5000 laser shots. The red arrow indicates the wavelength λ(online) ~ 297.79 nm used for the time-resolved kinetic studies of CH$_3$O$_2$.

action (R3) reacted further with NO before the fluorescence detection:

$$CH_3O + NO \rightarrow CH_2O + HNO, \tag{R10}$$

$$CH_3O + NO + M \rightarrow CH_3ONO + M, \tag{R11}$$

where M = N$_2$, O$_2$. In addition to the above reactions, CH$_3$O reacts with O$_2$ by Reaction (R4). Figure 4 shows the dependence of the LIF signal on the concentration of NO obtained experimentally and by numerical simulations using Reactions (R3)–(R4) and (R10)–(R11) and outlined in the Supplement. A maximum signal was obtained with
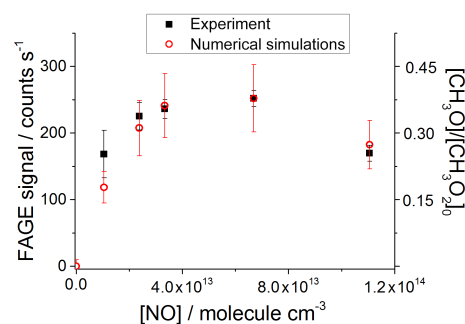
Figure 4. FAGE signal (left axis) and the ratio [CH$_3$O] / [CH$_3$O$_2$]$_0$ (right axis) as a function of the concentration of NO for a reaction time of 3 ms. Black squares are experimental CH$_3$O signals (errors are 1σ) and red circles are the ratio [CH$_3$O] / [CH$_3$O$_2$]$_0$ generated by numerical simulations (percentage uncertainties are 20 %) using the chemistry system outlined in the main text and described in further detail in the Supplement.

added [NO] = 6.7×10^{13} molecule cm^{-3} for a reaction time of 3 ms, estimated from the linear flow velocity within the FAGE reactor. Figure 4 shows that the functional dependence with added [NO] of the experimental CH$_3$O signal and the simulated [CH$_3$O] / [CH$_3$O$_2$]$_0$ ratio display the same shape (within overlapping error limits), with the numerical simulations showing that [CH$_3$O] / [CH$_3$O$_2$]$_0$ at the detection axis was ~ 0.4 (i.e. 40 % conversion to CH$_3$O).

2.3 FAGE calibrations

CH$_3$O and CH$_3$O$_2$ calibrations were carried out using the conventional radical source, employed in fieldwork for OH and HO$_2$ calibrations (Heard and Pilling, 2003), that produces radicals in a flow tube impinging just outside the FAGE inlet pinhole (Winiberg et al., 2015) and is described in Sect. 2.3.1. Two methods of calibration have been used for CH$_3$O$_2$: the flow-tube method and the kinetics of the self-reaction of CH$_3$O$_2$ carried out in HIRAC.

2.3.1 Calibration for methoxy radicals

In the CH$_3$O calibration experiments, nitrogen (BOC, > 99.998 %) was used as carrier gas. Part of the N$_2$ flow was passed through a methanol (Sigma Aldrich, $\geq$ 99.9 %) bubbler while the other portion bypassed the bubbler. The gas containing methanol vapour was then passed through a square-cross-section flow tube of dimensions 13×13 mm (internal) and 300 mm length with a flow rate of 40 slm (ensuring turbulent flow conditions), controlled by an electronic flow controller (Brooks, 0–100 slm air). The collimated light of a Hg Pen-Ray lamp (LOT-Oriel, Hg(Ar)) was directed across the flow tube (close to the downstream end) to photolyse methanol vapour. The flow-tube output was impinged close to the FAGE inlet to sample CH$_3$O radicals at atmospheric pressure through a 1 mm diameter pinhole (Fig. 1).

The concentration of CH$_3$O radicals was calculated using Eq. (1):

$$[CH_3O] = [CH_3OH]\sigma_{CH_3OH,\,184.9\,nm}$$
$$\Phi_{CH_3O,\,184.9\,nm} F_{184.9\,nm} \Delta t, \qquad (1)$$

where $\sigma_{CH_3OH,\,184.9\,nm}$ is the absorption cross section of methanol at 184.9 nm, $(6.35 \pm 0.28) \times 10^{-19}$ cm^2 molecule^{-1}, obtained by averaging reported values (Dillon et al., 2005; Jimenez et al., 2003; Nee et al., 1985); $F_{184.9\,nm}$ is the photon flux of 184.9 nm light; and Δt is the irradiation time of the gas. Although it is known, based on end-product analysis, that the scission of the O–H bond is a major photolysis channel of methanol at 184.9 nm (Buenker et al., 1984; Porter and Noyes, 1959), the photodissociation quantum yield of CH$_3$O at 184.9 nm, $\Phi_{CH_3O,\,184.9\,nm}$, has not yet been reported. Here it is assumed that $\Phi_{CH_3O,\,184.9\,nm}$ is equal to the photodissociation quantum yield at 193.3 nm, $\Phi_{CH_3O,\,193.3\,nm} = 0.86 \pm 0.10$, which has been reported (Satyapal et al., 1989). In order to determine the methanol vapour concentration in the flow tube, [CH$_3$OH], separate experiments were carried out with the same calibration system to bubble deionised water instead of methanol with the same flow rate. The water vapour concentration, [H$_2$O], was measured using a dew-point hygrometer (CR4, Buck Research Instruments) prior to the flow tube. Then [CH$_3$OH] was calculated using the averaged [H$_2$O] and the vapour pressures p_{CH_3OH} and p_{H_2O} at the temperatures measured for CH$_3$OH (13 °C) and H$_2$O (15 °C) in the bubbler:

$$[CH_3OH] = [H_2O]\frac{p_{CH_3OH}}{p_{H_2O}}. \qquad (2)$$

Equation (2) assumes that there were no losses of water vapour and methanol vapour by condensation in the tubing connecting the bubbler to the flow tube. This is as expected based on the small difference in temperature between the bubbler (vide supra) and the connecting tubing (typically held at ~20 °C) and as the gas going through the bubbler was diluted with the gas bypassing the bubbler.

N$_2$O photolysis at 184.9 nm to generate NO (via reaction of the photoproduct (O^{1}D) with N$_2$O giving a known yield of NO), which was subsequently measured using a commercial analyser, was used as a chemical actinometer to obtain the product $F_{184.9\,nm} \times \Delta t$ (Winiberg et al., 2015) and hence calculate [CH$_3$O] via Eq. (1). The photolysis time, Δt, was estimated to be 8.3 ms, using the volumetric flow rate and the geometric parameters of the flow tube (assuming plug flow), and was in turn used to determine $F_{184.9\,nm}$. Although it is the product $F_{184.9\,nm} \times \Delta t$ which is used to calculate [CH$_3$O], any change in the volumetric flow rate between the calibration and actinometry experiments will change Δt, and hence the product was corrected for any changes in volumetric flow rate. A range of [CH$_3$O] at constant [CH$_3$OH] was produced by changing the electrical current through the Hg lamp be-

tween 0 and 20 mA, and hence $F_{184.9\,nm}$, to generate the calibration plot presented in Fig. 5.

2.3.2 Calibration for methyl peroxy radicals

Flow-tube method

Methyl peroxy radicals were generated by water photolysis at 184.9 nm (Reaction R7) to give OH, followed by the reaction with excess methane in air (BOC, synthetic BTCA 178) – Reactions (R1)–(R2) to give CH$_3$O$_2$. The calibrations were performed using the set-up described above. Methane (BOC, CP grade, 99.5 %) was flowed at 82.5 sccm to convert OH into CH$_3$, which subsequently reacted rapidly with O$_2$ to form CH$_3$O$_2$. Figure S1 (Supplement) shows an example of the OH signal with and without CH$_4$. The signal in the presence of CH$_4$ was 0.04 ± 0.04 of the signal in the absence of CH$_4$ showing that 0.96 ± 0.04 of OH was converted into CH$_3$O$_2$. The result is in agreement with the estimation of the fraction of OH titrated to CH$_3$O$_2$, 0.97, using a rate coefficient of 6.4×10^{-15} cm^3 molecule^{-1} s^{-1} for the OH + CH$_4$ reaction (Atkinson et al., 2006) and an average residence time of OH in the calibration flow tube of 11 ms determined using the volumetric flow rate and the geometric parameters of the flow tube and position of the Hg pen lamp.

The concentration of CH$_3$O$_2$ was determined using Eq. (3):

$$[CH_3O_2] = 0.96[OH] = 0.96[H_2O]\sigma_{H_2O,\,184.9\,nm}$$
$$\Phi_{H_2O,\,184.9\,nm} F_{184.9\,nm} \Delta t, \qquad (3)$$

where $\sigma_{H_2O,\,184.9\,nm}$ is the absorption cross section of water vapour at 184.9 nm, $(7.22 \pm 0.22) \times 10^{-20}$ cm^2 molecule^{-1} (Cantrell et al., 1997; Creasey et al., 2000), and $\Phi_{H_2O,\,184.9\,nm}$ is the photodissociation quantum yield of OH, which is equal to unity. The values of $F_{184.9\,nm}$ and Δt were determined as described in the Sect. 2.3.1. No loss of CH$_3$O$_2$ by reaction with the HO$_2$ radicals generated by the reaction of H atoms with O$_2$ (Reaction R8) was encountered over the residence time of the radicals in the calibration flow tube (~11 ms) as CH$_3$O$_2$ reacts with HO$_2$ on a 10 s timescale as determined using a reaction rate coefficient of 5.2×10^{-12} cm^3 molecule^{-1} s^{-1} (Atkinson et al., 2006) and the radical concentrations in the flow tube. The CH$_3$O$_2$ radicals sampled through the FAGE pinhole expansion to a pressure of 2.65 Torr reached the detection region in about 85 ms, while the calculated CH$_3$O$_2$ + HO$_2$ reaction half-life at this reduced pressure in the FAGE inlet was thousands of seconds, and any change in the CH$_3$O$_2$ concentration is expected to be negligible.

Figure 6 shows results obtained from three separate calibration experiments. In the first two experiments air was humidified by passing a fraction of the air flow (40 slm total flow rate) through a deionised water bubbler. The hygrometer measured 7.5×10^{16} molecule cm^{-3} of water vapour prior to the calibration flow tube, and the concentration of methane
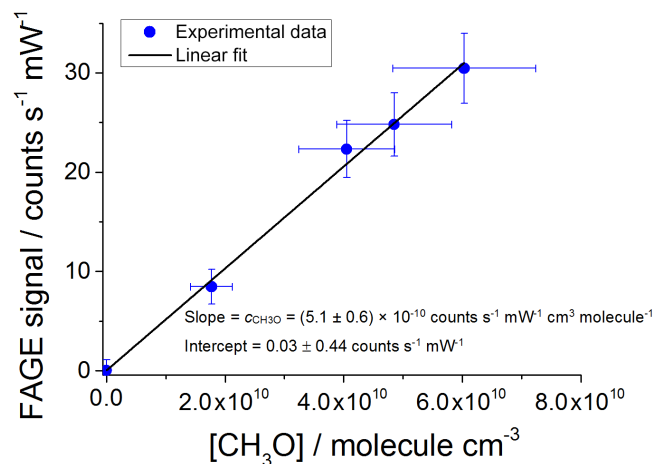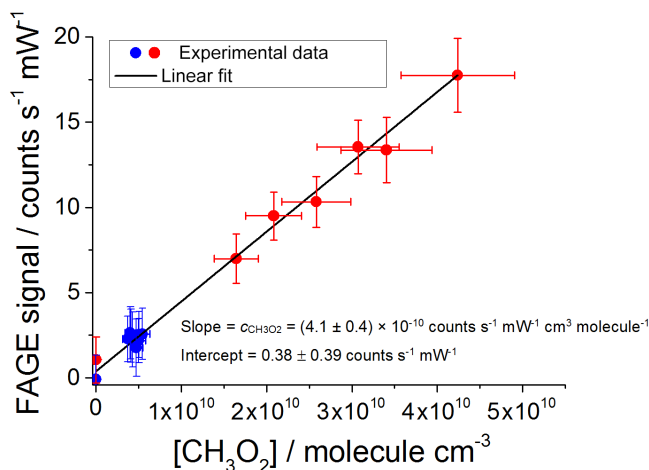
Figure 5. FAGE calibration for CH_3O at atmospheric pressure and 293 K; laser power $P = 12.9 \pm 0.3$ mW and pressure in the detection cell is 2.65 ± 0.05 Torr. The FAGE signal, including the measurement with the Hg lamp turned off ($[CH_3O] = 0$), was obtained after subtraction of the offline signal, 12.3 ± 0.9 counts s^{-1} mW^{-1}. Averaging time per point = 120 s. The error limits in $[CH_3O]$ and the FAGE signal for the x and y axes respectively are representative of the 1σ overall uncertainty, which contains the total systematic and statistical errors (see text for details of these). The error limits shown in the legend are the standard errors in the slope and intercept of the fit to the experimental data.

in the flow tube was 5×10^{16} molecule cm^{-3}. In the second experiment, a series of FAGE measurements were performed using a photon flux of $\sim 1.6 \times 10^{14}$ photon cm^{-2} s^{-1} to generate $\sim 4.5 \times 10^9$ molecule cm^{-3} CH_3O_2. In the third experiment $[CH_4] = 10^{17}$ molecule cm^{-3} and all the air flow (now at 20 slm) was passed through the water bubbler to obtain 3×10^{17} molecule cm^{-3} H_2O vapour. The concentration of CH_3O_2 was varied by changing the photon flux in the range of 0.5–1.5×10^{14} photon cm^{-2} s^{-1} to generate $[CH_3O_2] = 1.5$–4.5×10^{10} molecule cm^{-3}.

CH_3O_2 second-order decay method

The principle behind this calibration method is that the second-order decay of CH_3O_2 is dependent upon its initial concentration, and hence its quantification offers an alternative way to calibrate the signal. The experiments were performed in the HIRAC chamber at 295 K and 1 bar of synthetic air obtained by mixing high purity oxygen (BOC, $> 99.999\%$) and nitrogen (BOC, $> 99.998\%$) in the ratio of $O_2 : N_2 = 1 : 4$. Methane (BOC, CP grade, 2–3×10^{17} molecule cm^{-3}) and molecular chlorine (Sigma Aldrich, $\geq 99.5\%$, 0.3–2.1×10^{14} molecule cm^{-3}) were delivered to the chamber. Eight UV black lamps (Phillips, TL-D 36W/BLB, $\lambda = 350$–400 nm) housed in quartz tubes mounted radially inside the reactive volume were used to photolyse Cl_2 to generate Cl atoms and initiate the chem-

Figure 6. FAGE calibration for CH_3O_2 at atmospheric pressure and 293 K. The data were obtained by three separate experiments: two of them generating $[CH_3O_2] \cong 4.5 \times 10^9$ molecule cm^{-3} in the calibration flow tube (blue circles); laser power $P = 9.5 \pm 0.3$ mW and 11.6 ± 0.4 mW respectively and one experiment using $[CH_3O_2]$ in the range of 1.5–4.5×10^{10} molecule cm^{-3} (red circles); $P = 9.2 \pm 0.2$ mW. The pressure in the FAGE detection cell was maintained at 2.65 ± 0.05 Torr in all experiments. Averaging time per point = 120 s. The error limits in $[CH_3O_2]$ and the FAGE signal for the x and y axes respectively are representative for the 1σ overall uncertainty, which contains the total systematic and statistical errors. The error limits shown in the legend are the standard errors in the slope and intercept of the fit to the experimental data.

istry:

$$CH_4 + Cl \rightarrow CH_3 + HCl, \tag{R12}$$
$$CH_3 + O_2 + M \rightarrow CH_3O_2 + M. \tag{R2}$$

Numerical simulations using the chemical system described in Table S3 in the Supplement showed that $[Cl]_0 = 1$–6×10^6 molecule cm^{-3} (varied by changing the initial $[Cl_2]$). The high excess of methane (2–3×10^{17} molecule cm^{-3}) relative to $[Cl]_0$ ensured that the reactions of the Cl atoms with the self-reaction products formaldehyde and methanol were negligible. In each HIRAC experiment the lamps were alternatively turned on for 2–3 min and then off over 1–2 min to generate a series of typically 3–4 CH_3O_2 kinetic decays.

In order to detect CH_3O_2 the FAGE instrument was coupled to HIRAC through a custom-made ISO-K160 flange to sample the gas with a flow rate of ~ 3 slm. For most measurements, the 1 mm pinhole of the 280 mm long FAGE inlet sampled ~ 230 mm from the chamber wall as in the OH measurements reported previously (Winiberg et al., 2015). Additional investigations into any CH_3O_2 gradient across the ~ 600 mm radius of HIRAC were conducted using measurements of CH_3O_2 formed by the CH_4 reaction with O^1D generated by the photolysis of O_3 at 254 nm followed by the reaction of the produced CH_3 radical with O_2 at 295 K and 1 bar of synthetic air. An extended FAGE inlet (length

520 mm) was used to sample along 500 mm across the chamber starting with the inlet pinhole flush at the wall. A constant concentration of CH$_3$O$_2$ was found (within the 10 % overall error of the measurement) for all the sampled distances of 0–500 mm from the wall (note that 0 mm here refers to the FAGE inlet being at an equivalent position to the wall away from the mounting flange). The absence of a CH$_3$O$_2$ gradient across the chamber provides evidence of the efficacy of the mixing in HIRAC and shows that the wall loss of CH$_3$O$_2$ is negligible and hence that a shorter inlet, and hence distance from inlet to CH$_3$O$_2$ detection axis, could be used in future CH$_3$O$_2$ FAGE measurements within HIRAC, improving further the sensitivity.

2.4 Methoxy radical measurements within HIRAC

The experiment was carried out in HIRAC at 295 K and 1 bar of N$_2$ (BOC, > 99.998 %), but without any NO added to the FAGE cell (the cell furthest from the pinhole as shown in Fig. 1) so that [CH$_3$O] is measured directly. Initial concentrations in HIRAC were [CH$_4$]$_0$ = 4.50 × 10^{17} molecule cm^{-3} and [Cl$_2$]$_0$ = 5.57 × 10^{15} molecule cm^{-3}. After adding the reagents into the chamber, the lamps (vide supra) were turned on to generate CH$_3$O by Reaction (R6b).

3 Results

3.1 Sensitivity and detection limits for CH$_3$O$_2$ and CH$_3$O radicals obtained from calibrations

3.1.1 Flow-tube method

The FAGE sensitivity for CH$_3$O$_2$ ($C_{\text{CH}_3\text{O}_2}$) and CH$_3$O ($C_{\text{CH}_3\text{O}}$) is the slope of the linear regressions in Figs. 5 and 6, which were $C_{\text{CH}_3\text{O}_2}$ = (4.1 ± 1.4) × 10^{-10} counts cm^3 molecule^{-1} s^{-1} mW^{-1} and $C_{\text{CH}_3\text{O}}$ = (5.1 ± 2.2) × 10^{-10} counts cm^3 molecule^{-1} s^{-1} mW^{-1}. The error limits, 34 % for $C_{\text{CH}_3\text{O}_2}$ and 43 % for $C_{\text{CH}_3\text{O}}$, are the overall 2σ uncertainties calculated using the sum in quadrature of the systematic uncertainties, 33 % for CH$_3$O$_2$ and 42 % for CH$_3$O (details in Sect. 3.2.1), and the statistical errors from the calibration plots, ∼ 8 %. The higher errors in $C_{\text{CH}_3\text{O}}$ compared to $C_{\text{CH}_3\text{O}_2}$ are due to the uncertainty in the methanol concentration, which is not determined directly (vide supra), and the error in the yield of CH$_3$O from CH$_3$OH photolysis. The value of the CH$_3$O photolysis yield from CH$_3$OH reported at 193 nm was used (0.86 ± 0.10), which has an uncertainty of 12 % at the 1σ level (Satyapal et al., 1989).

From the sensitivity factor, C, the limit of detection (LOD) was calculated using Eq. (4) and assuming Poisson statistics appropriate for single photon counting:

$$\text{LOD}\,(\text{CH}_3\text{O}_2) = \frac{S/N}{C_{\text{CH}_3\text{O}_2}\,P}\sqrt{\frac{\text{BKG}}{t}\left(\frac{1}{m}+\frac{1}{n}\right)},$$

$$\text{LOD}\,(\text{CH}_3\text{O}) = \frac{S/N}{C_{\text{CH}_3\text{O}}\,P}\sqrt{\frac{\text{BKG}}{t}\left(\frac{1}{m}+\frac{1}{n}\right)}, \quad (4)$$

where S/N is the signal-to-noise ratio; P is the laser power; BKG is the background signal and had a typical value of ∼ 100 counts s^{-1}, which represents ∼ 50 counts s^{-1} laser-scattered light within the detection cell and ∼ 50 counts s^{-1} scattered visible light which enters the pinhole from the room with a negligible contribution (1 count s^{-1} on average) of the detector dark counts; t is the time per data point; m represents the number of online data points; and n is the number of offline data points. For a typical 5 min averaged signal, i.e. $m = n = 150$, $S/N = 2$, $P = 15$ mW and $t = 1$ s, and using the values of C from the calibration, LOD(CH$_3$O$_2$) = 3.8 × 10^8 molecule cm^{-3} and LOD(CH$_3$O) = 3.0 × 10^8 molecule cm^{-3}. An increase in the averaging time to 1 h, i.e. $m = n = 1800$ data points, results in a decrease in the detection limits to LOD(CH$_3$O$_2$) = 1.1 × 10^8 molecule cm^{-3} and LOD(CH$_3$O) = 8.7 × 10^7 molecule cm^{-3}.

Although CH$_3$O$_2$ has not been measured specifically in the atmosphere, there have been several calculations of its concentration using numerical models. In general, the concentration of CH$_3$O$_2$ is a function of both the loadings of VOCs and the levels of NO$_x$. For the clean, remote environments at Cape Verde in the tropical Atlantic Ocean and in the Borneo rainforest, [CH$_3$O$_2$] is calculated to peak around 6 × 10^8 molecule cm^{-3} and about 2 × 10^8 molecule cm^{-3} respectively at noon using the modelling studies reported by Whalley et al. (2010, 2011). Therefore, it should be possible using the FAGE conversion method for CH$_3$O$_2$ with an averaging time of 1 h (vide supra) to achieve a measurement of atmospheric levels of CH$_3$O$_2$ in such clean environments, and shorter averaging times in some cases. Further optimisations of FAGE sensitivity can be achieved by the removal of the fibre optic cables to deliver the probe laser beam directly to the CH$_3$O detection cell to increase the laser power and by increasing the pulse repetition frequency above the current value of 5 kHz (but without significant reduction in the pulse energy). The present investigations into the change of sensitivity with pressure in the range from 2.65 to 10.00 Torr found that 2.65 Torr is the optimum value in this pressure interval. The result suggests that, by reducing the pressure in the above range of values, the decrease in fluorescence due to the reduction in the CH$_3$O number density was overcome by the increase in the fluorescence quantum yield due to a lower fluorescence quenching rate. Another reason could be that the characteristics of the jet expansion and/or the ensuing flow to the LIF detection region change with pressure, leading to a more favourable transmission of radicals to the

detection region, but it is difficult to test this experimentally. Hence an additional improvement in the sensitivity might be obtained by using a lower detection cell pressure than the current value of 2.65 Torr using a more powerful pump. It should be also noted that the distance from the inlet pinhole to the laser axis in the CH$_3$O and CH$_3$O$_2$ fluorescence cell (Fig. 1, ~ 580 mm) is considerably longer than the corresponding distance in the ground-based field fluorescence cell for OH and HO$_2$ detection (88 mm), and improvements in sensitivity would be expected for a shorter pinhole-to-laser excitation distance for CH$_3$O$_2$. The further optimisations of sensitivity and the planned construction of a reference cell to find the online wavelength position could potentially enable CH$_3$O$_2$ measurements to be made in urban environments where CH$_3$O$_2$ concentrations are estimated to be considerably lower – for example a few 10^7 molecule cm^{-3} based on modelling results (Whalley et al., 2017).

The calibrations using the flow-tube ("wand") method have been performed under water vapour concentrations similar to the ambient [H$_2$O$_{vapour}$] but a few orders of magnitude higher than those present in the HIRAC chamber experiments. In contrast with [H$_2$O$_{vapour}$], the methane concentrations used in the "wand" method were similar to [CH$_4$] present in HIRAC but higher than [CH$_4$] in the atmosphere. However, as detailed in this paragraph, the effects of methane and water vapour on our sensitivity are minimal. Estimations using the reported fluorescence quenching rate coefficient of CH$_3$O(A) by CH$_4$, $k_{quench.CH_4} = 1.05 \times 10^{-10}$ cm^3 molecule^{-1} s^{-1}, (Wantuck et al., 1987) and the concentrations of CH$_4$ in the LIF detection cell for the calibrations using the flow tube (1.7×10^{14} and 3.4×10^{14} molecule cm^{-3}, corresponding to 5.0×10^{16} and 1.0×10^{17} molecule cm^{-3} respectively in the flow tube) resulted in only ~ 1–2 % lower fluorescence quantum yield compared to the value determined in the absence of CH$_4$. No literature value has been found for the quenching rate coefficient of CH$_3$O(A) fluorescence by H$_2$O vapour. However, even if it assumed to be as large as the above-reported value for CH$_4$ ($k_{quench.CH_4}$), only a few percent decrease in the fluorescence quantum yield is computed (compared with a water concentration of zero) for the levels of H$_2$O vapour which are present at the CH$_3$O$_2$ FAGE detection axis when using the "wand" calibration method. These levels (1–2 % v/v) are similar to a typical water vapour concentration in the atmosphere. A very good agreement has been obtained between the calibration factors for CH$_3$O$_2$ detection with two different concentrations of water vapour in the flow tube: 7.5×10^{16} or 3.0×10^{17} molecule cm^{-3} (corresponding to 2.6×10^{14} and 1.0×10^{15} molecule cm^{-3} respectively in the FAGE cell) as shown in Fig. 6 in Sect. 2.3.2. This very good agreement for H$_2$O vapour and the above calculations for CH$_4$ support the use of the flow-tube method for the FAGE calibration of the CH$_3$O$_2$ concentrations.

3.1.2 Methyl peroxy calibration using kinetics of the CH$_3$O$_2$ second-order decay

An alternative method of calibration for CH$_3$O$_2$ was to generate CH$_3$O$_2$ radicals in HIRAC to monitor the temporal decay of the CH$_3$O$_2$ FAGE signal once the photolysis lamps were turned off. Figure 7 shows an example of a decay in the CH$_3$O$_2$ signal generated by extinguishing the HIRAC lamps following the production of CH$_3$O$_2$ by the Cl-atom-initiated oxidation of CH$_4$ in the presence of O$_2$ (Reactions R12 and R2). In the absence of other processes, the loss of CH$_3$O$_2$ is described by the integrated second-order rate law equation describing the CH$_3$O$_2$ self-reaction (Reaction R6):

$$\frac{1}{[CH_3O_2]_t} = \frac{1}{[CH_3O_2]_0} + 2 \cdot k_{obs}t, \qquad (5)$$

where [CH$_3$O$_2$]$_t$ is the methyl peroxy concentration at reaction time t, [CH$_3$O$_2$]$_0$ is the initial concentration when the lights are switched off and k_{obs} is the observed rate coefficient (which is not equal to k_6, see below). Using [CH$_3$O$_2$] = $\frac{S_{CH_3O_2}}{C_{CH_3O_2}}$, where $S_{CH_3O_2}$ is the signal measured by FAGE and $C_{CH_3O_2}$ is the instrument sensitivity, Eq. (6) is obtained for the temporal profile of the methyl peroxy signal:

$$\frac{1}{(S_{CH_3O_2})_t} = \frac{1}{(S_{CH_3O_2})_0} + \frac{2 \cdot k_{obs}t}{C_{CH_3O_2}} \quad \text{or}$$

$$(S_{CH_3O_2})_t = 1 / \left(\frac{1}{(S_{CH_3O_2})_0} + \frac{2 \cdot k_{obs}t}{C_{CH_3O_2}} \right), \qquad (6)$$

In Eq. (6) $(S_{CH_3O_2})_t$ and $(S_{CH_3O_2})_0$ are the signal at time t and $t = 0$ respectively.

Equation (6) was fitted to the experimental decays of $S_{CH_3O_2}$ (see Fig. 7 as an example) fixing k_{obs} to the IUPAC recommendation, $k_{obs} = (4.8 \pm 1.1) \times 10^{-13}$ cm^3 molecule^{-1} s^{-1}, in order to obtain $C_{CH_3O_2}$. Eighteen CH$_3$O$_2$ decays were analysed, which yielded an average value of $C_{CH_3O_2} = (5.6 \pm 1.7) \times 10^{-10}$ counts cm^3 molecule^{-1} s^{-1} mW^{-1}. The error limit, 30 %, is the 2σ composite error calculated as the sum in quadrature of the total systematic uncertainty, 29 % (see Sect. 3.2.2), and the average random error of all determinations, with 8 %, taken as two standard errors in the fit of Eq. (6) to the CH$_3$O$_2$ temporal decays. This value agrees well with $C_{CH_3O_2} = (4.1 \pm 1.4) \times 10^{-10}$ counts cm^3 molecule^{-1} s^{-1} mW^{-1} obtained from the flow-tube calibration method (Sect. 3.1.1).

Based on the lack of a measurable CH$_3$O$_2$ radical gradient across HIRAC (Sect. 2.3.2., vide supra), it is assumed that the loss of CH$_3$O$_2$ to the walls of HIRAC in these experiments was negligible over the timescale of 1–2 min of the temporal decay measurements. Our finding is consistent with previous results showing that the heterogeneous wall-loss rates for CH$_3$O$_2$ were significantly lower than the corresponding removal rates of HO$_2$ (Miyazaki et al., 2010; Mihele et al., 1999; Fuchs et al., 2008). Using a 30 cm long
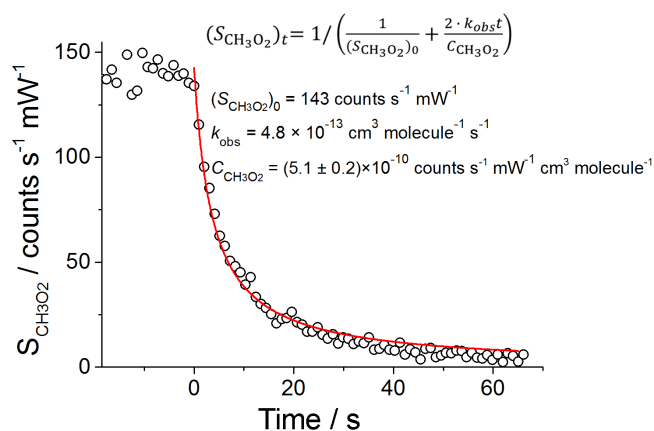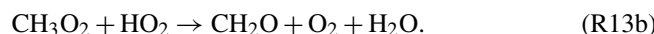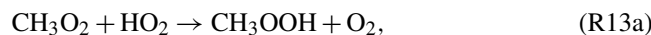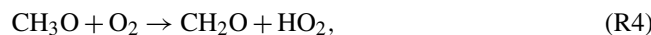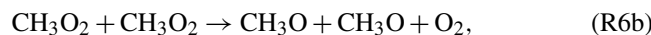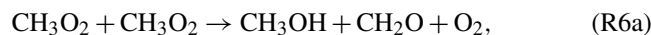
Figure 7. Second-order decay of the normalized CH_3O_2 signal with 1 s time resolution generated in HIRAC using $Cl/CH_4/O_2$ and black lamps (see main text for details); $[CH_4]_0 = 2.3 \times 10^{17}$ molecule cm^{-3} and $[Cl_2]_0 = 5.8 \times 10^{13}$ molecule cm^{-3} at 295 K and 1 bar mixture of $N_2 : O_2 = 4 : 1$. At time zero the lamps were turned off. Fitting Eq. (6) to the data yielded $C_{CH_3O_2} = (5.1 \pm 0.2) \times 10^{-10}$ counts cm^3 molecule^{-1} s^{-1} mW^{-1} (statistical error at 1σ level).

glass tube of 2 cm diameter, Miyazaki et al. (2010) measured that the heterogeneous removal efficiency for CH_3O_2 was 6 times lower than for HO_2. The HO_2 wall-loss rate coefficient at room temperature and 1000 mbar in HIRAC was found to be of $\sim 10^{-2}$ s^{-1} (Winiberg et al., 2015). Therefore, it can be expected that the wall-loss rate coefficient of CH_3O_2 in HIRAC was $k_{loss} \cong 10^{-3}$ s^{-1} and so is not considered in the analysis here for CH_3O_2 decays which typically last for ~ 100 s. In order to investigate the sensitivity of $C_{CH_3O_2}$ obtained by the kinetic analysis of the CH_3O_2 decay to k_{loss} higher than 10^{-3} s^{-1}, a wall-loss rate coefficient of 10^{-2} s^{-1} was included in the analysis of the experimental decays of CH_3O_2 to obtain $C_{CH_3O_2}$, but only an increase in $C_{CH_3O_2}$ of about 6 % on average was seen. A small deviation of the experimental data from the fit was obtained at the end of the measurements whether or not k_{loss} was included in the analysis (Fig. 7). The role of potential secondary chemistry at later times of the reaction will be investigated in future kinetic studies of the CH_3O_2 self-reaction.

Using the average sensitivity factor $C_{CH_3O_2} = (5.6 \pm 1.7) \times 10^{-10}$ counts cm^3 molecule^{-1} s^{-1} mW^{-1} determined by the CH_3O_2 decay method in HIRAC, and for a signal-to-noise ratio $S/N = 2$, a laser power $P = 15$ mW and a time per data point $t = 1$ s in Eq. (4) results in an improved (compared with the flow-tube calibration) $LOD(CH_3O_2) = 2.8 \times 10^8$ molecule cm^{-3} for 5 min averaging time, i.e. 150 online data points (m) and 150 offline points (n). The corresponding LOD for an averaging time of 1 h, i.e. $m = n = 1800$, is $LOD(CH_3O_2) = 7.9 \times 10^7$ molecule cm^{-3}.

It should be noted that the observed rate coefficient, k_{obs}, is larger than the second-order rate coefficient of just the

CH_3O_2 recombination Reaction (R6), k_6, as the methoxy radicals generated by channel R6b react rapidly with molecular oxygen present in large excess, 5×10^{18} molecule cm^{-3}, to produce HO_2 (Reaction R4) which in turn reacts with CH_3O_2 (Reaction R13):

$$CH_3O_2 + CH_3O_2 \rightarrow CH_3OH + CH_2O + O_2, \tag{R6a}$$
$$CH_3O_2 + CH_3O_2 \rightarrow CH_3O + CH_3O + O_2, \tag{R6b}$$
$$CH_3O + O_2 \rightarrow CH_2O + HO_2, \tag{R4}$$
$$CH_3O_2 + HO_2 \rightarrow CH_3OOH + O_2, \tag{R13a}$$
$$CH_3O_2 + HO_2 \rightarrow CH_2O + O_2 + H_2O. \tag{R13b}$$

As each HO_2 radical consumes one CH_3O_2 species (Reaction R13) on the timescale of Reaction (R6), k_{obs} is given by (Sander and Watson, 1981; Lightfoot et al., 1990)

$$k_{obs} = k_6 (1 + r_{6b}), \tag{7}$$

where r_{6b} is the branching ratio for the reaction channel R6b. According to IUPAC (Atkinson et al., 2006), there is a 23 % uncertainty in k_{obs} of the CH_3O_2 recombination at 298 K with a recommended value $k_{obs} = 4.8 \times 10^{-13}$ cm^3 molecule^{-1} s^{-1}. This value corresponds to $k_6 = (3.5 \pm 1.0) \times 10^{-13}$ cm^3 molecule^{-1} s^{-1} and $r_{6b} = 0.37 \pm 0.06$ (Atkinson et al., 2006).

In order to check the validity of Eq. (7) in the presence of HO_2 removal by self-reaction and wall loss, numerical simulations were performed to generate CH_3O_2 decays using a system incorporating the chemistry described by Reactions (R4), (R6), (R13) and (R14) (vide infra) and a heterogeneous loss of HO_2, $k_{loss(HO_2)}$ (see Supplement). The rate coefficients were sourced from the preferred IUPAC value at 298 K (Table S3 in Supplement) and $k_{loss(HO_2)}$ was varied. The simulated decays of $[CH_3O_2]$ vs. time were analysed using Eq. (5) (see Fig. S3 as an example) and gave an average observed rate coefficient of $k_{obs} = 4.7 \times 10^{-13}$ cm^3 molecule^{-1} s^{-1}, which is only 2 % lower than the IUPAC recommendation, for $k_{loss(HO_2)}$ varied between 0.01 and 0.10 s^{-1}, and, hence confirm the applicability of Eq. (7).

$$HO_2 + HO_2 \rightarrow H_2O_2 + O_2 \tag{R14a}$$
$$HO_2 + HO_2 + M \rightarrow H_2O_2 + O_2 + M \tag{R14b}$$
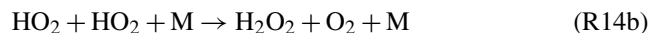
3.2 Calibration uncertainties

3.2.1 Flow-tube method

The 2σ error associated with $C_{CH_3O_2}$ of 34 % obtained by the flow-tube method ($C_{CH_3O_2} = (4.1 \pm 1.4) \times 10^{-10}$ counts cm^3 molecule^{-1} s^{-1} mW^{-1}) represents the overall uncertainty calculated using the sum in quadrature of the systematic uncertainty, 33 %, and the statistical error from the calibration plots, ~ 8 %. The overall 34 % uncertainty is similar to the previous estimated total uncertainty,

36 %, in the use of the same method for calibration of OH and HO$_2$ measurements in HIRAC, where no CH$_4$ is added (Winiberg et al., 2015). The flow-tube method is a proven method to generate known amounts of OH and HO$_2$ by the photolysis of H$_2$O at 184.9 nm in order to calibrate field instruments (Heard and Pilling, 2003).

The largest contribution to the total error of the method came from the 28 % total uncertainty in the photon flux of the calibration source, $F_{184.9nm}$. The product $F_{184.9nm} \times \Delta t$ is determined using N$_2$O actinometry relying on the measurement of [NO] in trace amounts (0.2–1.5 ppbv) using a commercial NO analyser (Thermo Electron Corporation 42C) followed by the data analysis using four rate coefficients each with $\sim$ 10 % uncertainty (Burkholder et al., 2015). Although it is the product $F_{184.9nm} \times \Delta t$ which is directly determined by the actinometric method and used to calculate the concentration of radicals to calibrate FAGE (Eq. 3), any difference in the volumetric flow rate between the calibration and actinometry experiments will change Δt. Therefore, the uncertainty in Δt, 2 %, needs to be accounted for. The contributions from the rest of the terms in Eq. (3) to the systematic uncertainty in the determination of [CH$_3$O$_2$] by this method were as follows: 6 % total error in $\sigma_{H_2O, 184.9nm}$ (Cantrell et al., 1997); 10 % uncertainty in [H$_2$O], taken from the instrumental uncertainty of the hygrometer; and 4 % error in the yield of CH$_3$O$_2$ produced by the OH conversion into CH$_3$ followed by the CH$_3$ + O$_2$ reaction. The contribution of the uncertainties in the FAGE measurements to the 33 % overall systematic uncertainty in the calibration were estimated to consist of 12 % in the online FAGE signal and 6 % uncertainty in the laser power measured by the laser power meter and used to normalise the data. The uncertainty associated with the online signal, 12 % at 2σ level, was calculated as the average deviation of the signal value due to the error limits of $\pm 5 \times 10^{-4}$ nm in the online wavelength position (see the typical laser excitation scans shown in Fig. 3).

3.2.2 CH$_3$O$_2$ second-order decay calibration

The largest contribution to the calculated overall 2σ uncertainty of 30 % in $C_{CH_3O_2}$ obtained by the CH$_3$O$_2$ second-order decay method ($C_{CH_3O_2} = (5.6 \pm 1.7) \times 10^{-10}$ counts cm^3 molecule^{-1} s^{-1} mW^{-1}) derives from the 23 % error in the IUPAC-preferred value of the observed rate coefficient for the effective CH$_3$O$_2$ self-reaction, $k_{obs} = (4.8 \pm 1.1) \times 10^{-13}$ cm^3 molecule^{-1} s^{-1} (Atkinson et al., 2006). It is instructive to examine the origin of the 23 % error. The studies which led to the IUPAC recommendation utilised the UV absorption of CH$_3$O$_2$, typically at 250 nm, and the determined quantity was the ratio between the observed rate coefficient and the absorption cross section of CH$_3$O$_2$, k_{obs}/σ_{250nm}. IUPAC and the Jet Propulsion Laboratory (JPL) recommend 3.9×10^{-18} and 3.8×10^{-18} cm^2 molecule^{-1} respectively for σ_{250nm} (Atkinson et al., 2006; Burkholder et al., 2015). The JPL recommendation (Burkholder et al.,

2015) is the cross section obtained by the re-evaluation of the previous reported UV-absorption spectra by Tyndall et al. (2001) in 2001 (Tyndall et al., 2001), yielding $\sigma_{250nm} = 3.78 \times 10^{-18}$ cm^2 molecule^{-1}. Tyndall et al. (2001) used a cross section of $(4.26 \pm 0.52) \times 10^{-18}$ cm^2 molecule^{-1} (error at 2σ) for the maximum at 237.3 nm, obtained by analysing the shape of the absorption spectra between 200 and 300 nm reported since 1990. The studies before 1990 were not included due to errors in the calibration of the CH$_3$O$_2$ cross section leading to large discrepancies in the reported values. The 2001 evaluation of Tyndall et al. (2001) calculated $k_{obs} = (4.7 \pm 0.8) \times 10^{-13}$ cm^3 molecule^{-1} s^{-1}, where the error limits are two standard deviations of the mean. Including an error of 10 % in the cross section of CH$_3$O$_2$, as suggested by the authors (Tyndall et al., 2001), a 19 % composite uncertainty in k_{obs} is obtained. The result is in good agreement with the 23 % uncertainty in the IUPAC recommendation.

The remaining contributions to the uncertainty in the calibration using the CH$_3$O$_2$ second-order decay method are a 6 % error in the laser power, 12 % uncertainty in the online signal determined by how well the laser is able to find the online wavelength position (vide supra) and 10 % error in $(S_{CH_3O_2})_0$ in Eq. (6), which is the value of the CH$_3$O$_2$ signal at the moment when the HIRAC lamps were turned off to generate a second-order decay.

3.2.3 Comparison between the FAGE sensitivities for CH$_3$O$_2$ obtained by the two calibration methods

The FAGE sensitivity factor obtained using the flow-tube method, $C_{CH_3O_2} = (4.1 \pm 1.4) \times 10^{-10}$ counts cm^3 molecule^{-1} s^{-1} mW^{-1}, is 27 % lower but has overlapping error limits with the result found using the CH$_3$O$_2$ second-order decay method, $C_{CH_3O_2} = (5.6 \pm 1.7) \times 10^{-10}$ counts cm^3 molecule^{-1} s^{-1} mW^{-1} (uncertainties quoted to 2σ). The calculated overall error in the CH$_3$O$_2$ second-order decay method, 30 %, is similar to the total uncertainty in the flow-tube method, 34 %. The flow-tube method is known to reliably generate accurate concentrations of radicals and has been used for many years in the calibration of FAGE instruments employed in field measurements of OH and HO$_2$ (Heard and Pilling, 2003). The flow-tube method has also been validated by using alternate methods of calibration, for example using the decay of a hydrocarbon in the HIRAC chamber to obtain [OH] (Winiberg et al., 2015). The method of using a time-resolved kinetic quantity to derive a calibration factor was validated for HO$_2$ in HIRAC, where C_{HO_2} obtained from analysis of the temporal decay of HO$_2$ agreed with C_{HO_2} from the flow-tube method (Winiberg et al., 2015). These results suggests that the sensitivity of the FAGE system, represented by the value of C, is not changed between sampling from the calibration flow tube and sampling from within HIRAC itself.

The accuracy of the CH$_3$O$_2$ temporal decay method is largely determined by the accuracy of k_{obs} (see Sect.3.2.2. above). The quantity measured in the previous kinetic studies of CH$_3$O$_2$+ CH$_3$O$_2$ is $k_{obs}/\sigma_{250\,nm}$ and hence the accuracy of k_{obs} is directly affected by any systematic errors in the determination of $\sigma_{250\,nm}$. In order to make $C_{CH_3O_2}$ derived from the temporal decay and flow-tube methods of the same, the value of k_{obs} would need to be reduced by $\sim 25\%$, which in turn requires a $\sim 25\%$ reduction in $\sigma_{250\,nm}$. It is noted that the UV-absorption spectrum of CH$_3$O$_2$ is relatively broad and hence may prevent a selective detection due to the difficulty in discriminating from the potential presence of other species also absorbing around 250 nm, such as Cl$_2$ and CH$_3$CHO used in concentrations as high as 10^{16} molecule cm^{-3}, while [CH$_3$O$_2$] was $\sim 10^{13}$ molecule cm^{-3} (Dagaut and Kurylo, 1990; Roehl et al., 1996). As the absorption cross sections of Cl$_2$ and CH$_3$CHO at 250 nm lay in the range 10^{-21}–10^{-22} cm^2 molecule^{-1} (Keller-Rudek et al., 2013), the unaccounted for absorption of these species may have led to an overestimation of $\sigma_{250\,nm}$(CH$_3$O$_2$).

As noted in the 2001 review by Tyndall et al. (2001), none of the previous laboratory studies of the CH$_3$O$_2$ recombination measured [CH$_3$O$_2$] by any method other than UV-spectroscopy. In addition, the traditional time-resolved measurements of CH$_3$O$_2$ used high CH$_3$O$_2$ concentrations (10^{13}–10^{15} molecule cm^{-3}) and, as the self-reaction is fairly slow, Tyndall et al. (2001) stated that the results were potentially affected by secondary chemistry (Tyndall et al., 2001). Therefore, there is a need for the use of a complementary technique in the kinetic study of this reaction, for example by LIF as described in this paper, which may offer some advantages to probe CH$_3$O$_2$ selectively in the absence of interferences from other species. In addition, LIF is more sensitive and hence requires significantly lower radical concentrations ([CH$_3$O$_2$]$_0$ = (1–3) × 10^{11} molecule cm^{-3} here) than the UV-absorption studies, which may help to minimise potential secondary chemistry.

3.3 Methoxy radical measurement within HIRAC

The typical concentration of [O$_2$] = 5 × 10^{18} molecule cm^{-3} used in the HIRAC experiments described above was lowered in some experiments to decrease the consumption of CH$_3$O by O$_2$ via Reaction (R4). In this manner, a concentration of methoxy radicals was obtained above the FAGE limit of detection in HIRAC to enable a direct measurement over a few minutes. The chamber was filled with high purity nitrogen ($> 99.998\%$), but the ~ 6 m long N$_2$ delivery pipe was purposely incompletely purged before the experiment in order to deliver trace levels of oxygen to HIRAC. The initial Cl$_2$ concentration in these experiments was 5.6 × 10^{15} molecule cm^{-3} and hence was 1–2 orders of magnitude higher than [Cl$_2$]$_0$ used in the kinetic experiments above in order to generate higher [Cl] and hence [CH$_3$O]. The concentration

of CH$_3$O during the experiment was computed by using the FAGE calibration factor for methoxy radicals generated from the photolysis of methanol in N$_2$, $C_{CH_3O} = (5.1 \pm 2.2) \times 10^{-10}$ counts cm^3 molecule^{-1} s^{-1} mW^{-1} (Sect. 3.1.1). The temporal profile of CH$_3$O is shown in Fig. 8, together with a numerical simulation of CH$_3$O(t), using a chemistry system described in the Supplement. The best fit to the experimental CH$_3$O concentration profile was obtained for [O$_2$] = (5.4 ± 0.6) × 10^{15} molecule cm^{-3}, i.e. around 0.02 % relative to N$_2$. The numerical simulations showed that Cl$_2$ consumption was dominated by the reaction with CH$_3$ radicals, present at a relatively high concentration, explaining the $\sim 50\%$ decrease in [CH$_3$O] observed during its temporal measurement shown in Fig. 8. The Supplement (Fig. S5) shows the concentration profiles of Cl$_2$, Cl, CH$_3$ and CH$_3$O$_2$ obtained by numerical simulations performed over ~ 2 min.

These results demonstrate the capability to measure an absolute concentration of CH$_3$O radicals in a simulation chamber, with CH$_3$O representing a further model target species for the validation of chemical mechanisms for the chemical oxidation of VOCs. However, it is recognised that the experiments need to be performed at reduced [O$_2$] and that [O$_2$] needs to be known a priori in order to test robustly the accuracy of the chemical mechanism and underlying kinetic parameters.

4 Conclusions

Currently there is no measurement of the absolute concentration of CH$_3$O$_2$ radicals in the atmosphere. In this work the FAGE technique has been extended by adding the capability to detect CH$_3$O$_2$ and CH$_3$O radicals to the more typical measurement of OH and HO$_2$ radicals. The method enables the speciated and sensitive detection of CH$_3$O$_2$ radicals by converting CH$_3$O$_2$ into CH$_3$O by reaction with NO and detecting the resultant CH$_3$O by LIF with excitation at ca. 298 nm. The limit of detection of the method obtained using the radical source commonly employed to provide accurate concentrations of OH with added CH$_4$ is 3.8 × 10^8 molecule cm^{-3} for a signal-to-noise ratio of 2 and 5 min time resolution and reduces to 1.1 × 10^8 molecule cm^{-3} for $S/N = 2$ and 1 h averaging time. Therefore, the method has the potential to be used in field measurements of the diurnal profiles of CH$_3$O$_2$ in clean air with low NO$_x$ levels, such as remote continental environments and in the marine boundary layer. Further improvements of the FAGE sensitivity could be achieved via the increase in the laser repetition frequency above the current value of 5 kHz, a decrease in the detection chamber pressure (currently ~ 2.65 Torr), and the use of a shorter distance between the inlet sampling pinhole and the fluorescence detection axis (presently a long distance of ~ 580 mm). The method is also demonstrated for the direct detection of CH$_3$O, in the absence of added NO to the fluorescence cell.
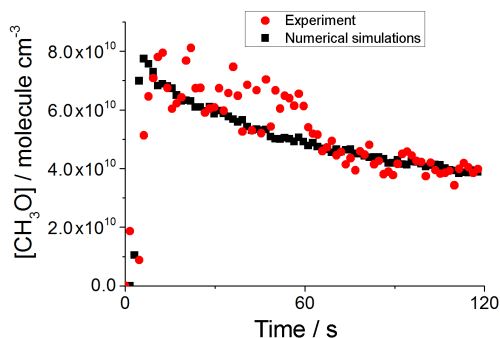
Figure 8. Concentration of CH$_3$O as a function of time in HIRAC: red points are the experimental data and black points are generated by a numerical simulation. CH$_3$O radicals were formed as a product of the self-reaction of CH$_3$O$_2$ species at 295 K and 1 bar of N$_2$, with CH$_3$O$_2$ generated by the reaction of Cl atoms with CH$_4$, and with the HIRAC black lamps being turned on at time zero. Oxygen was present in trace amounts, determined to be $(5.4 \pm 0.6) \times 10^{15}$ molecule cm^{-3} from comparison of the simulations to the experimental data. The chemical mechanism used in the numerical simulations is presented in the Supplement.

The limit of detection for CH$_3$O determined using the conventional radical source for $S/N = 2$ and 5 min averaging time is 3.0×10^8 molecule cm^{-3}.

Additional investigations into the FAGE sensitivity for CH$_3$O$_2$ were carried out in the HIRAC simulation chamber at Leeds, by studying the kinetics of the second-order decays of CH$_3$O$_2$ by its self-reaction. The second-order decays of CH$_3$O$_2$ were analysed by fixing the observed rate coefficient to the IUPAC recommendation, $k_{obs} = (4.8 \pm 1.1) \times 10^{-13}$ cm^3 molecule^{-1} s^{-1} (Atkinson et al., 2006), in the fitting routine to extract the FAGE sensitivity factor for CH$_3$O$_2$, $C_{CH_3O_2}$. The obtained value, $C_{CH_3O_2} = (5.6 \pm 0.9) \times 10^{-10}$ counts cm^3 molecule^{-1} s^{-1} mW^{-1}, agrees well with the result found using the conventional radical source, $C_{CH_3O_2} = (4.1 \pm 0.7) \times 10^{-10}$ counts cm^3 molecule^{-1} s^{-1} mW^{-1} (uncertainties quoted to 1σ). The two values have overlapping error limits at 1σ level.

In addition to the quantitative detection of CH$_3$O$_2$, experiments were carried out to measure CH$_3$O generated as a product by the CH$_3$O$_2$ self-reaction in HIRAC. Oxygen was present at a significantly lower concentration to reduce the consumption rate of CH$_3$O by reaction with O$_2$ in order to enable the measurement. Good agreement between the experimental data and [CH$_3$O] generated by numerical simulations using a model describing the chemical system was obtained, demonstrating the capability to quantitatively measure CH$_3$O. In addition to CH$_3$O$_2$, a measurement of CH$_3$O will be useful as a further model target in future mechanistic studies of atmospherically relevant chemical systems within HIRAC.

The Supplement related to this article is available online at https://doi.org/10.5194/amt-10-3985-2017-supplement.

References

Albaladejo, J., Jimenez, E., Notario, A., Cabanas, B., and Martinez, E.: CH$_3$O yield in the CH$_3$ + O$_3$ reaction using the LP/LIF technique at room temperature, J. Phys. Chem. A, 106, 2512–2519, https://doi.org/10.1021/jp012249o, 2002.

Atkinson, R., Baulch, D. L., Cox, R. A., Crowley, J. N., Hampson, R. F., Hynes, R. G., Jenkin, M. E., Rossi, M. J., Troe, J., and IUPAC Subcommittee: Evaluated kinetic and photochemical data for atmospheric chemistry: Volume II – gas phase reactions of organic species, Atmos. Chem. Phys., 6, 3625–4055, https://doi.org/10.5194/acp-6-3625-2006, 2006.

Biggs, P., Canosa-Mas, C. E., Fracheboud, J. M., Parr, A. D., Shallcross, D. E., Wayne, R. P., and Caralp, F.: Investigation into the pressure dependence between 1 and 10 Torr of the reactions of NO$_2$ with CH$_3$ and CH$_3$O, J. Chem. Soc. Faraday T., 89, 4163–4169, https://doi.org/10.1039/ft9938904163, 1993.

Biggs, P., Canosa-Mas, C. E., Fracheboud, J. M., Shallcross, D. E., and Wayne, R. P.: Kinetics of the reaction of F atoms with CH$_3$ONO and CH$_3$O, and the reaction of CH$_3$O with a number of hydrocarbons, J. Chem. Soc. Faraday T., 93, 2481–2486, https://doi.org/10.1039/a701175j, 1997.

Bossolasco, A., Farago, E. P., Schoemaecker, C., and Fittschen, C.: Rate constant of the reaction between CH$_3$O$_2$ and OH radicals, Chem. Phys. Lett., 593, 7–13, https://doi.org/10.1016/j.cplett.2013.12.052, 2014.

Buenker, R. J., Olbrich, G., Schuchmann, H. P., Schurmann, B. L., and Vonsonntag, C.: Photolysis of methanol at 185 nm. Quantum mechanical calculations and product study, J. Am. Chem. Soc., 106, 4362–4368, https://doi.org/10.1021/ja00328a011, 1984.

Burkholder, J. B., Sander, S. P., Abbatt, J. P. D., Barker, J. R., Huie, R. E., Kolb, C. E., Kurylo, M. J., Orkin, V. L., Wilmouth, D. M., and Wine, P. H.: Chemical kinetics and photochemical data for

use in atmospheric studies – Evaluation No. 18, JPL Publication 15-10, available at: http://jpldataeval.jpl.nasa.gov/ (last access: 22 February 2017), 2015.

Cantrell, C. A. and Stedman, D. H.: A possible technique for the measurement of atmospheric peroxy-radicals, Geophys. Res. Lett., 9, 846–849, https://doi.org/10.1029/GL009i008p00846, 1982.

Cantrell, C. A., Stedman, D. H., and Wendel, G. J.: Measurement of atmospheric peroxy-radicals by chemical amplification, Anal. Chem., 56, 1496–1502, https://doi.org/10.1021/ac00272a065, 1984.

Cantrell, C. A., Zimmer, A., and Tyndall, G. S.: Absorption cross sections for water vapor from 183 to 193 nm, Geophys. Res. Lett., 24, 2195–2198, https://doi.org/10.1029/97gl02100, 1997.

Chai, J. J., Hu, H. Y., Dibble, T. S., Tyndall, G. S., and Orlando, J. J.: Rate Constants and Kinetic Isotope Effects for Methoxy Radical Reacting with NO_2 and O_2, J. Phys. Chem. A, 118, 3552–3563, https://doi.org/10.1021/jp501205d, 2014.

Chen, Y., Yang, C., Zhao, W., Fang, B., Xu, X., Gai, Y., Lin, X., Chen, W., and Zhang, W.: Ultra-sensitive measurement of peroxy radicals by chemical amplification broadband cavity-enhanced spectroscopy, Analyst, 141, 5870–5878, https://doi.org/10.1039/c6an01038e, 2016.

Creasey, D. J., Heard, D. E., and Lee, J. D.: Absorption cross-section measurements of water vapour and oxygen at 185 nm. Implications for the calibration of field instruments to measure OH, HO_2 and RO_2 radicals, Geophys. Res. Lett., 27, 1651–1654, https://doi.org/10.1029/1999gl011014, 2000.

Dagaut, P. and Kurylo, M. J.: The gas phase UV absorption spectrum of CH_3O_2 radicals: A reinvestigation, J. Photoch. Photobio. A, 51, 133–140, https://doi.org/10.1016/1010-6030(90)87047-f, 1990.

Dillon, T. J., Holscher, D., Sivakumaran, V., Horowitz, A., and Crowley, J. N.: Kinetics of the reactions of HO with methanol (210–351 K) and with ethanol (216–368 K), Phys. Chem. Chem. Phys., 7, 349–355, https://doi.org/10.1039/b413961e, 2005.

Ebata, T., Yanagishita, H., Obi, K., and Tanaka, I.: A-X Fluorescence-Spectra of CH_3O and C_2H_5O Generated by the ArF Laser Photolysis of Alkyl Nitrites, Chem. Phys., 69, 27–33, https://doi.org/10.1016/0301-0104(82)88129-9, 1982.

Edwards, G. D., Cantrell, C. A., Stephens, S., Hill, B., Goyea, O., Shetter, R. E., Mauldin, R. L., Kosciuch, E., Tanner, D. J., and Eisele, F. L.: Chemical ionization mass spectrometer instrument for the measurement of tropospheric HO_2 and RO_2, Anal. Chem., 75, 5317–5327, https://doi.org/10.1021/ac034402b, 2003.

Farago, E. P., Viskolcz, B., Schoemaecker, C., and Fittschen, C.: Absorption Spectrum and Absolute Absorption Cross Sections of CH_3O_2 Radicals and CH_3I Molecules in the Wavelength Range 7473–7497 cm^{-1}, J. Phys. Chem. A, 117, 12802–12811, https://doi.org/10.1021/jp408686s, 2013.

Fuchs, H., Holland, F., and Hofzumahaus, A.: Measurement of tropospheric RO_2 and HO_2 radicals by a laser-induced fluorescence instrument, Rev. Sci. Instrum., 79, 084104, https://doi.org/10.1063/1.2968712, 2008.

Glowacki, D. R., Goddard, A., Hemavibool, K., Malkin, T. L., Commane, R., Anderson, F., Bloss, W. J., Heard, D. E., Ingham, T., Pilling, M. J., and Seakins, P. W.: Design of and initial results from a Highly Instrumented Reactor for Atmo-

spheric Chemistry (HIRAC), Atmos. Chem. Phys., 7, 5371–5390, https://doi.org/10.5194/acp-7-5371-2007, 2007.

Green, T. J., Reeves, C. E., Fleming, Z. L., Brough, N., Rickard, A. R., Bandy, B. J., Monks, P. S., and Penkett, S. A.: An improved dual channel PERCA instrument for atmospheric measurements of peroxy radicals, J. Environ. Monitor., 8, 530–536, https://doi.org/10.1039/b514630e, 2006.

Hanke, M., Uecker, J., Reiner, T., and Arnold, F.: Atmospheric peroxy radicals: ROXMAS, a new mass-spectrometric methodology for speciated measurements of HO_2 and ΣRO_2 and first results, Int. J. Mass Spectrom., 213, 91–99, https://doi.org/10.1016/s1387-3806(01)00548-6, 2002.

Heard, D. E. and Pilling, M. J.: Measurement of OH and HO_2 in the troposphere, Chem. Rev., 103, 5163–5198, https://doi.org/10.1021/cr020522s, 2003.

Hernandez, M. D. A., Burkert, J., Reichert, L., Stobener, D., Meyer-Arnek, J., Burrows, J. P., Dickerson, R. R., and Doddridge, B. G.: Marine boundary layer peroxy radical chemistry during the AEROSOLS99 campaign: Measurements and analysis, J. Geophys. Res.-Atmos., 106, 20833–20846, https://doi.org/10.1029/2001jd900113, 2001.

Inoue, G., Akimoto, H., and Okuda, M.: Laser-induced fluorescence spectra of CH_3O, Chem. Phys. Lett., 63, 213–216, https://doi.org/10.1016/0009-2614(79)87002-5, 1979.

Inoue, G., Akimoto, H., and Okuda, M.: Spectroscopy of the CH_3O A^2A_1–X ^2E system by laser-excited fluorescence method, J. Chem. Phys., 72, 1769–1775, https://doi.org/10.1063/1.439291, 1980.

Jenkin, M. E., Cox, R. A., Hayman, G. D., and Whyte, L. J.: Kinetic study of the reactions $CH_3O_2 + CH_3O_2$ and $CH_3O_2 + HO_2$ using molecular modulation spectroscopy, J. Chem. Soc. Farad. T. 2, 84, 913–930, https://doi.org/10.1039/f29888400913, 1988.

Jenkin, M. E., Young, J. C., and Rickard, A. R.: The MCM v3.3.1 degradation scheme for isoprene, Atmos. Chem. Phys., 15, 11433–11459, https://doi.org/10.5194/acp-15-11433-2015, 2015.

Jimenez, E., Gilles, M. K., and Ravishankara, A. R.: Kinetics of the reactions of the hydroxyl radical with CH_3OH and C_2H_5OH between 235 and 360 K, J. Photoch. Photobio. A, 157, 237–245, https://doi.org/10.1016/s1010-6030(03)00073-x, 2003.

Kappert, J. and Temps, F.: Rotationally resolved laser-induced fluorescence excitation studies of CH_3O, Chem. Phys., 132, 197–208, https://doi.org/10.1016/0301-0104(89)80088-6, 1989.

Kassab, E., Gleghorn, J. T., and Evleth, E. M.: Theoretical aspects of the photochemistry of methanol, methylamine, and related materials, J. Am. Chem. Soc., 105, 1746–1753, https://doi.org/10.1021/ja00345a008, 1983.

Keller-Rudek, H., Moortgat, G. K., Sander, R., and Sörensen, R.: The MPI-Mainz UV/VIS Spectral Atlas of Gaseous Molecules of Atmospheric Interest, Earth Syst. Sci. Data, 5, 365–373, https://doi.org/10.5194/essd-5-365-2013, 2013.

Kurylo, M. J. and Wallington, T. J.: The temperature dependence of the rate constant for the gas phase disproportionation reaction of CH_3O_2 radicals, Chem. Phys. Lett., 138, 543–547, https://doi.org/10.1016/0009-2614(87)80121-5, 1987.

Lightfoot, P. D., Lesclaux, R., and Veyret, B.: Flash photolysis study of the $CH_3O_2 + CH_3O_2$ reaction: Rate constants and branching ratios from 248 to 573 K, J. Phys. Chem., 94, 700–707, https://doi.org/10.1021/j100365a035, 1990.

Malkin, T. L., Goddard, A., Heard, D. E., and Seakins, P. W.: Measurements of OH and HO$_2$ yields from the gas phase ozonolysis of isoprene, Atmos. Chem. Phys., 10, 1441–1459, https://doi.org/10.5194/acp-10-1441-2010, 2010.

Marston, C. C., Weide, K., Schinke, R., and Suter, H. U.: Product selectivity of vibrationally mediated photofragmentation of methanol, J. Chem. Phys., 98, 4718–4727, https://doi.org/10.1063/1.464976, 1993.

McAdam, K., Veyret, B., and Lesclaux, R.: UV absorption spectra of HO$_2$ and CH$_3$O$_2$ radicals and the kinetics of their mutual reactions ant 298 K, Chem. Phys. Lett., 133, 39–44, https://doi.org/10.1016/0009-2614(87)80049-0, 1987.

Mihele, C. M., Mozurkewich, M., and Hastie, D. R.: Radical loss in a chain reaction of CO and NO in the presence of water: Implications for the radical amplifier and atmospheric chemistry, Int. J. Chem. Kinet., 31, 145–152, https://doi.org/10.1002/(sici)1097-4601(1999)31:2<145::aid-kin7>3.0.co;2-m, 1999.

Miyazaki, K., Parker, A. E., Fittschen, C., Monks, P. S., and Kajii, Y.: A new technique for the selective measurement of atmospheric peroxy radical concentrations of HO$_2$ and RO$_2$ using a denuding method, Atmos. Meas. Tech., 3, 1547–1554, https://doi.org/10.5194/amt-3-1547-2010, 2010.

Nagesh, J., Sibert, E. L., and Stanton, J. F.: Simulation of A^{2}A$_1$ <-X^{2}E laser excitation spectrum of CH$_3$O and CD$_3$O, Spectrochim. Acta A, 119, 90–99, https://doi.org/10.1016/j.saa.2013.02.037, 2014.

Nee, J. B., Suto, M., and Lee, L. C.: Photoexcitation processes of CH$_3$OH: Rydberg states and photofragment fluorescence, Chem. Phys., 98, 147–155, https://doi.org/10.1016/0301-0104(85)80102-6, 1985.

Orlando, J. J. and Tyndall, G. S.: Laboratory studies of organic peroxy radical chemistry: an overview with emphasis on recent issues of atmospheric significance, Chem. Soc. Rev., 41, 8213–8213, 2012.

Porter, R. P. and Noyes, W. A.: Photochemical studies, LIV. Methanol vapor, J. Am. Chem. Soc., 81, 2307–2311, https://doi.org/10.1021/ja01519a007, 1959.

Powers, D. E., Pushkarsky, M. B., and Miller, T. A.: Rovibronic analysis of the laser induced fluorescence excitation spectrum of the jet-cooled methoxy radical, J. Chem. Phys., 106, 6863–6877, https://doi.org/10.1063/1.473712, 1997.

Roehl, C. M., Bauer, D., and Moortgat, G. K.: Absorption spectrum and kinetics of the acetylperoxy radical, J. Phys. Chem., 100, 4038–4047, https://doi.org/10.1021/jp9526298, 1996.

Sander, S. P. and Watson, R. T.: Kinetic studies of the reactions of CH$_3$O$_2$ with NO, NO$_2$ and CH$_3$O$_2$ at 298 K, J. Phys. Chem., 84, 1664–1674, https://doi.org/10.1021/j100450a002, 1980.

Sander, S. P. and Watson, R. T.: Temperature dependence of the self-reaction of CH$_3$O$_2$ radicals, J. Phys. Chem., 85, 2960–2964, https://doi.org/10.1021/j150620a023, 1981.

Satyapal, S., Park, J., Bersohn, R., and Katz, B.: Dissociation of methanol and ethanol activated by a chemical-reaction or by light, J. Chem. Phys., 91, 6873-6879, https://doi.org/10.1063/1.457356, 1989.

Saunders, S. M., Jenkin, M. E., Derwent, R. G., and Pilling, M. J.: Protocol for the development of the Master Chemical Mechanism, MCM v3 (Part A): tropospheric degradation of non-aromatic volatile organic compounds, Atmos. Chem. Phys., 3, 161–180, https://doi.org/10.5194/acp-3-161-2003, 2003.

Shannon, R. J., Blitz, M. A., Goddard, A., and Heard, D. E.: Accelerated chemistry in the reaction between the hydroxyl radical and methanol at interstellar temperatures facilitated by tunnelling, Nat. Chem., 5, 745–749, https://doi.org/10.1038/nchem.1692, 2013.

Simon, F. G., Schneider, W., and Moortgat, G. K.: UV absorption spectrum of the methylperoxy radical and the kinetics of its disproportionation reaction at 300 K, Int. J. Chem. Kinet., 22, 791–812, https://doi.org/10.1002/kin.550220802, 1990.

Tyndall, G. S., Wallington, T. J., and Ball, J. C.: FTIR product study of the reactions CH$_3$O$_2$ + CH$_3$O$_2$ and CH$_3$O$_2$ + O$_3$, J. Phys. Chem. A, 102, 2547–2554, https://doi.org/10.1021/jp972784h, 1998.

Tyndall, G. S., Cox, R. A., Granier, C., Lesclaux, R., Moortgat, G. K., Pilling, M. J., Ravishankara, A. R., and Wallington, T. J.: Atmospheric chemistry of small organic peroxy radicals, J. Geophys. Res.-Atmos., 106, 12157–12182, https://doi.org/10.1029/2000jd900746, 2001.

Wantuck, P. J., Oldenborg, R. C., Baughcum, S. L., and Winn, K. R.: Collisional quenching of CH$_3$O (A ^{2}A$_1$), J. Phys. Chem., 91, 3253–3259, https://doi.org/10.1021/j100296a030, 1987.

Wen, Y., Segall, J., Dulligan, M., and Wittig, C.: Photodissociation of methanol at 193.3 nm: Translational energy release spectra, J. Chem. Phys., 101, 5665–5671, https://doi.org/10.1063/1.467352, 1994.

Wendt, H. R. and Hunziker, H. E.: Electronic absorption spectrum of CH$_3$O, J. Chem. Phys., 71, 5202–5205, https://doi.org/10.1063/1.438296, 1979.

Whalley, L. K., Furneaux, K. L., Goddard, A., Lee, J. D., Mahajan, A., Oetjen, H., Read, K. A., Kaaden, N., Carpenter, L. J., Lewis, A. C., Plane, J. M. C., Saltzman, E. S., Wiedensohler, A., and Heard, D. E.: The chemistry of OH and HO$_2$ radicals in the boundary layer over the tropical Atlantic Ocean, Atmos. Chem. Phys., 10, 1555–1576, https://doi.org/10.5194/acp-10-1555-2010, 2010.

Whalley, L. K., Edwards, P. M., Furneaux, K. L., Goddard, A., Ingham, T., Evans, M. J., Stone, D., Hopkins, J. R., Jones, C. E., Karunaharan, A., Lee, J. D., Lewis, A. C., Monks, P. S., Moller, S. J., and Heard, D. E.: Quantifying the magnitude of a missing hydroxyl radical source in a tropical rainforest, Atmos. Chem. Phys., 11, 7223–7233, https://doi.org/10.5194/acp-11-7223-2011, 2011.

Whalley, L. K., Blitz, M. A., Desservettaz, M., Seakins, P. W., and Heard, D. E.: Reporting the sensitivity of laser-induced fluorescence instruments used for HO$_2$ detection to an interference from RO$_2$ radicals and introducing a novel approach that enables HO$_2$ and certain RO$_2$ types to be selectively measured, Atmos. Meas. Tech., 6, 3425–3440, https://doi.org/10.5194/amt-6-3425-2013, 2013.

Whalley, L. K., Stone, D., Hopkins, J., Holmes, R., Lee, J. D., Hamilton, J., and Heard, D. E.: Understanding in situ ozone production in the summertime through radical observations and modelling studies during the Clean air for London project, to be submitted, 2017.

Winiberg, F. A. F., Smith, S. C., Bejan, I., Brumby, C. A., Ingham, T., Malkin, T. L., Orr, S. C., Heard, D. E., and Seakins, P. W.: Pressure-dependent calibration of the OH and HO$_2$ channels of a FAGE HO$_x$ instrument using the Highly Instrumented Reactor

for Atmospheric Chemistry (HIRAC), Atmos. Meas. Tech., 8, 523–540, https://doi.org/10.5194/amt-8-523-2015, 2015.

Winiberg, F. A. F., Dillon, T. J., Orr, S. C., Groß, C. B. M., Bejan, I., Brumby, C. A., Evans, M. J., Smith, S. C., Heard, D. E., and Seakins, P. W.: Direct measurements of OH and other product yields from the $HO_2 + CH_3C(O)O_2$ reaction, Atmos. Chem. Phys., 16, 4023–4042, https://doi.org/10.5194/acp-16-4023-2016, 2016.

Zador, J., Taatjes, C. A., and Fernandes, R. X.: Kinetics of elementary reactions in low-temperature autoignition chemistry, Prog. Energ. Combust., 37, 371–421, https://doi.org/10.1016/j.pecs.2010.06.006, 2011.